The International Journal of Advanced Manufacturing Technology (2019) 100:457–473
https://doi.org/10.1007/s00170-018-2718-y

ORIGINAL ARTICLE

Experimental evaluation of surface topographies of NMQL grinding ZrO_2 ceramics combining multiangle ultrasonic vibration

Dongzhou Jia[1,2] · Changhe Li[1] · Yanbin Zhang[1] · Min Yang[1] · Xianpeng Zhang[1] · Runze Li[3] · Heju Ji[4]

Received: 22 June 2018 / Accepted: 17 September 2018 / Published online: 25 September 2018

Abstract

Nanofluid minimum quantity lubrication (NMQL) technique has many technological and economic advantages in grinding operation. NMQL can improve grinding performance in terms of cooling and lubrication and is ecofriendly because it consumes a small amount of grinding fluid. Ultrasonic machining can improve grinding performance owing to its reciprocating vibration mechanism and furrow widening. Consequently, the simultaneous utilization of these techniques is anticipated to improve the surface quality, especially for hard brittle materials. In this research, multiangle two-dimensional (2D) ultrasonic vibration is utilized in zirconia ceramic grinding. Results reveal that the adhesion and material peeling phenomenon on the workpiece surface is obviously reduced compared with dry grinding without ultrasonic vibration. The synergistic effect of multiangle 2D ultrasonic and NMQL is also studied. With increased angle, the roughness value is found to initially increase (from 45° to 90°) and then decreases (from 90° to 135°). Moreover, the lubricating effect under 90° is the poorest, with the highest *R*a and *RS*m values of 0.703 μm and 0.106 mm, respectively; conversely, the minimum *R*a value (0.585 μm) is obtained under 45°, and the lowest *RS*m value (0.076 mm) is obtained under 135°.

Keywords Zirconia ceramics · Surface grinding · 2D ultrasonic vibration · Nanofluid · Minimum quantity lubrication

Nomenclature

MQL	Minimum quantity lubrication
NMQL	Nanofluid minimum quantity lubrication
UAG	Ultrasonic-assisted grinding
ZTA	Zirconium toughening alumina
ZrO_2	Zirconia

Highlights

1. Multiangle ultrasonic vibration grinding performance with and without NMQL was studied.
2. The cutting mechanism of multiangle ultrasonic vibration was analyzed.
3. The simultaneous utilization of 2D ultrasonic vibration and NMQL mechanism was studied.
4. The surface quality was analyzed under different conditions.

✉ Changhe Li
sy_lichanghe@163.com

✉ Yanbin Zhang
zhangyanbin1_qdlg@163.com

Dongzhou Jia
jia_dongzhou@163.com

Min Yang
yummy0lige@163.com

Xianpeng Zhang
zhangxianpeng_mt@163.com

Runze Li
runzeli@usc.edu

Heju Ji
Jhj-8@163.com

[1] School of Mechanical Engineering, Qingdao University of Technology, Qingdao 266520, China

[2] School of Mechanical Engineering, Inner Mongolia University for Nationalities, Tongliao 028000, China

[3] Department of Biomedical Engineering, University of Southern California, Los Angeles, CA 90089–1111, USA

[4] Qingdao Dongjia Textile Machinery Group., Ltd, Qingdao 266520, China

Ra	Profile arithmetic average deviation
RSm	Average width of profile unit
v_w	Feed speed (m/min)
SEM	Scanning electron microscope
θ	The angle between axial and tangential ultrasonic vibratory
v_s	Peripheral speed of grinding wheel (m/s)
CG	Conventional grinding
MoS_2	Molybdenum disulfide
TZP	Tetragonal zirconium polycrystal
CNT	Carbon nanotube
A	Tangential amplitude (μm)
B	Axial amplitude (μm)
f	Ultrasonic vibration frequency (Hz)
φ	The difference of initial phase angle

1 Introduction

The superior mechanical and optical properties and biocompatibility of zirconia result in its extensive application in fields such as engineering and medicine. However, the flexural strength and breaking tenacity of zirconia are low [1]. Considerable research has been conducted on the machining process of difficult-to-machine materials (e.g., titanium alloy, nickel-based alloy, and ceramics) and their removal mechanism [2–6]. However, zirconia ceramic machining quality still remains to be improved, especially for grinding processes with extremely adverse working conditions in the cutting zone [7]. To improve the surface quality of the ceramic workpiece in the grinding process, researchers have implemented enormous exploratory works and believe that ultrasonic vibration can be used to effectively improve the surface quality and machining precision of hard brittle materials [8, 9]. Ultrasonic-assisted grinding (UAG) refers to the act of adding small-amplitude and high-frequency vibration to the tool or/and workpiece, so that it can realize the small-amplitude movement in one direction. The tool/workpiece results to linear reciprocal vibration (one-dimensional ultrasonic vibration-assisted grinding, 1D UAG) or elliptical vibration (two-dimensional ultrasonic vibra tion-assisted grinding, 2D UAG) under the effect of driving force. Selection of the proper combination of machining parameters like cutting speed, vibration amplitude, vibration frequency, and cutting depth can effectively reduce the cutting force. Compared with traditional cutting mode, ultrasonic-assisted machining can effectively improve finished surface precision and lengthen the service life of the tool [10].

Researchers have carried out a large quantity of research work on machining parameters, service life of the grinding wheel, and economic benefit in ultrasonic-assisted grinding process. Results show that compared with traditional grinding, the influences of various machining parameters in ultrasonic vibration are more complicated, but more ideal service life of grinding wheel and workpiece surface quality are commonly obtained [11, 12]. Researchers have carried out experimental studies on hard brittle materials, composite materials, difficult-to-machine materials, and new-type advanced materials; results show that ultrasonic-assisted machining can effectively improve the cutting performance of the above materials to obtain more ideal machining effect [13–15]. Yan [16] has studied the surface formation mechanism, material removal mechanism, and surface quality of nanozirconium toughening alumina ceramics (ZTA nanocomposite ceramics) under 2D UAG, and she analyzed how 2D ultrasonic vibration affects the processing characteristic of ZTA nanocomposite ceramics, which may reveal an efficient precision finishing characteristic of ZTA nanocomposite ceramics under 2D UAG and provide a fundamental basis for the popularization of 2D UAG. Tian [17] discussed the modeling method based on smoothed particle hydrodynamics method, simulated the process of single abrasive grain impacting ceramic workpiece, and built four types of single abrasive grain cutting processes, i.e., conventional grinding (CG), 3D UAG, axial, and vertical ultrasonic-assisted grinding. Zhou et al. [18] carried out the UAG tests of optical glass BK7 and analyzed the mechanism of subsurface crack damages. The experimental and analytical results show that the maximum depth of subsurface cracks is decreased obviously with the increase of spindle speed and ultrasonic vibration amplitude and a decrease in feel speed and grinding depth. Zhang et al. [19] used diamond micro abrasive tools to compare the surface quality of quartz glass under conventional grinding and ultrasonic-assisted micro grinding. The experimental results demonstrate that the grinding force is remarkably reduced by ultrasonic assistance. At the same time, the effect of grinding parameters on the grinding force is inhabited, and ductile machining is easier to be achieved, and surface quality is obviously improved due to ultrasonic assistance. Liu et al. [20] conducted comparative grinding experiments on pressureless sintered silicon materials by ultrasonic-assisted grinding and normal grinding methods. Then, the action mechanism of UAG was studied. The experimental results show that brittle fracture is the main removal mode in the grinding process. Under the same grinding parameters, the high-frequency impact of ultrasonic vibration-assisted grinding improves the fracture performance of the material, and the subsurface damage is suppressed to some extent. Ding et al. [21] conducted UAG and conventional grinding (CG, without ultrasonic) tests on carbon fiber-reinforced silicon carbide matrix (C/SiC) composites. The analysis was done by comparing the machining quality, grinding force, and specific grinding energy between the two processes. In comparison with CG, the normal grinding force and tangential grinding force for UAG were reduced maximally by 45 and 39% respectively, and the specific grinding energy was also reduced. Therefore, UAG can remarkably improve the grinding performance of C/SiC composites. The experiment by Li et al. [22] illustrates that

the grinding force increases with the increase of the grinding depth, feed rate, and amplitude, whereas it decreases with the increase of the spindle speed. The contrast experiment results show that UAG is beneficial for improving the surface quality and reducing the subsurface damage depth compared with common grinding.

Nik et al. [23] studied the ultrasonic vibration-assisted grinding of titanium alloy and found that the average grinding force and the tangential grinding force decreased by 13.5 and 14.2% respectively, and the surface roughness along the feed direction increased by 10%, which greatly improves the surface quality of the titanium alloy. Tawakoli et al. [24] compared the grinding performance of ultrasonic vibration auxiliary dry grinding and dry grinding for a soft material $42CrMo_4$ and found that ultrasonic-assisted dry grinding effectively reduced the surface roughness, normal grinding force, and heat damage, in which the normal grinding force decreased by 60%. Therefore, ultrasonic vibration can effectively enhance the grinding performance and improve the surface quality of the workpiece. Isobe et al. [25] applied the ultrasonic vibration to the mold to get the mirror grinding of the die steel. The vibration frequency was 60 kHz; the spindle speed was raised from 4000 to 9000 r/min; and the surface roughness *Rz* decreased to 0.14 μm. Abdullah et al. [26] analyzed the mechanism of abrasive grain and workpiece surface interaction of the ultrasonic vibration grinding. The results showed that a multiple and discontinuous cutting exists along the contact zone of the grinding wheel and the workpiece when longitudinal ultrasonic vibration was used. In conventional grinding, the grains move along a continuous arc, whereas under ultrasonic action, the cutting path is converted to a semi-sinusoidal curve. The application of ultrasonic vibration can effectively decrease the grinding force and avoid the thermal damage on the workpiece surface even without lubricant. Nomura et al. [27] examined the effect of ultrasonic vibration on the grinding force and surface roughness when the abrasive grain size and concentration of CBN grinding wheel are changed. The experimental results indicate that applying ultrasonic vibration to the wheel decreases the normal and tangential grinding forces by more than 50 and 78%, respectively, and improves the surface roughness by as much as 10% when the wheel abrasive grain size and concentration are changed. Over the range of the grinding conditions employed, the abrasive grain size as small as 5 μm can be used in ultrasonic-assisted grinding. Mahaddalkar et al. [28] studied the force and temperature effects in dry and flood grinding at vibration frequencies below ultrasonic. Based on a moving line heat source model, heat flux quantities were estimated from subsurface temperature measurements. Reductions in force of up to 30% were observed for dry grinding with 2360-Hz vibration assistance. For the same condition, the heat flux into the workpiece reduced by 42%. The present paper presents evidence that vibration assistance has a beneficial effect on the convective heat transfer rate.

Researchers have carried out a large number of research studies on cooling and lubrication in grinding, believing that NMQL is the most ideal clean and saving-type technique that can replace traditional lubrication [29–35]. NMQL is developed from MQL based on heat transfer enhancement theory. Nanoparticles are added in MQL to form a nanofluid that is atomized under the effect of compressed air to form small liquid droplets, which enter the grinding zone to achieve cooling and lubrication. Researchers deem that adding solid particles in base MQL can effectively improve its heat exchange capability and lower the temperature in the cutting zone [36–38]. With the development of nanoparticle materials science, researchers find that nanoparticles have unique properties compared with micro-order and quasi-micro-order particles, and NMQL is proposed based on this theory. Kalita et al. [39] added MoS_2 nanoparticles in paraffin oil and soybean oil for nanoparticle jet surface grinding experiments with cast iron and EN24 alloy steel. Through measuring and calculating grinding force, frictional coefficient, specific grinding energy, and G ratio, they verified the tribological properties of MoS_2 nanoparticles. They observed MoS_2 film formation on the abrasive grains of grinding wheel using SEM and analyzed the MoS_2 nanoparticle lubrication mechanism by measuring chemical elements on abrasive grains through energy spectrum. Lee et al. [40] conducted an experimental research on the MQL grinding and lubricating property of the nanofluid. Results revealed that nanofluid MQL prominently reduces the force and surface roughness. Moreover, ideal surface quality is obtained with smaller-sized nanoparticles. Mao et al. [41] used four different lubrication conditions (i.e., dry, flood, pure MQL, and Al_2O_3 nanofluid MQL) for grinding AISI52100. Results showed that water-based Al_2O_3 nanofluid MQL grinding exhibits optimal workpiece surface quality. Shen et al. [42] conducted grinding processing of cast iron and compared the process with dry grinding, flood grinding, and MQL. Results showed that nanoparticle jet flow MQL prominently reduces force and surface roughness, as well as effectively eliminates workpiece burning. The experiment simultaneously revealed that higher concentration of nanoparticles leads to higher G ratio. Zhang et al. [43, 44] studied the lubrication and cooling effects of different kinds of vegetable oils and analyzed the lubrication mechanism to a certain extent through NMQL grinding experiments. Simultaneously, Zhang et al. [45, 46] used the mixed nanofluids of MoS_2 and CNT to conduct the NMQL grinding of nickel-based alloy experiments, as well as analyzed the surface quality of the processed workpieces. The research showed that the NMQL of the mixed nanoparticles can provide more ideal lubrication for the grinding zone. When the nanoparticles have an average particle size of 50 nm and concentration of 6 wt%, optimum workpiece surface is obtained. Further, Zhang et al. [47] established the grinding force model under different lubrication conditions and achieved accurate prediction of grinding force. In order to improve the cooling ability of surgical skull

bone grinding, Yang et al. [48–50] sprayed the mist of medical nanofluid into the lesion area and developed a temperature field model of microscale bone grinding. The convective heat transfer and heat distribution coefficients under nanofluid MQL grinding are analyzed, and the excellent cooling effect of nanofluids is verified by theoretical analysis and experiment. Jia et al. [51] proved the lubrication effectiveness of the nanoparticles in the grinding zone by comparison with the flood grinding, MQL grinding, and dry grinding. They also discussed the optimum concentration of the nanoparticles. NMQL was found to obtain the best lubrication effect when the concentration of the nanoparticles was 6 wt%. Furthermore, Jia et al. [52] used a variety of vegetable oils for mixed vegetable oil NMQL grinding test. The results showed that the most ideal processing effect was obtained by adding MoS_2 nanoparticles with a mass fraction of 8 wt% in a mixture oil of soybean/castor. Jia et al. [53] reported that the best angle, pressure, and distance are 15°, 6 bar, and 10 mm, respectively, when NMQL technology was used to conduct plane grinding.

Although researchers have carried out a large quantity of research work on UAG and NMQL grinding, the research investigations on the combination of ultrasonic-assisted grinding parameters and lubricating conditions are not profound. Molaie et al. [54] combined MoS_2 nanofluid MQL to study the grinding force, force ratio, and surface roughness of 1D ultrasonic-assisted grinding. The results demonstrated that grinding force and surface roughness were obviously improved because tangential ultrasonic vibration exerted an important effect in the peak zone of the workpiece surface profile under abrasive grain cutting. The research conducted by Li et al. [9] indicated that, compared with traditional grinding, ultrasonic-assisted grinding can improve workpiece surface quality. Two different vibration frequencies were adopted in the experiment to investigate the effects of technological parameters on the surface quality and service life of the tool. Results showed that in ultrasonic-assisted grinding process, a small feed rate contributed to a more ideal surface when the frequency was 11.4 kHz. Meanwhile, the use of MQL was found to significantly lengthen the service life of the tool used in ultrasonic-assisted grinding.

Previous research work only compared grinding evaluation parameters under different lubricating conditions, such as grinding force, force ratio, and workpiece surface quality, without any in-depth analysis of the essential causes of the influence of the lubricating condition under ultrasonic vibration on machine quality. In addition, the present research studies on 2D ultrasonic-assisted grinding parameters did not involve the influence of ultrasonic vibrator angle on grinding quality. Based on the abovementioned facts, this paper studied grinding performances under multiangle conditions of tangential and axial vibrators, and analyzed the essential causes for nanofluid lubrication in the grinding zone under the effect of ultrasonic vibration based on further combination of nanofluid MQL lubrication.

2 Geometry and kinematics analyses of 2D ultrasonic vibrators

In 2D ultrasonic-assisted grinding, vertical installation mode is adopted for both ultrasonic vibrators; the angle is set as 90°, and directions are set as tangential (X-direction) and axial directions (Y-direction) along the grinding wheel. The two ultrasonic vibrators apply ultrasonic vibrations of certain amplitude and frequency in tangential and axial directions, which are usually driven by the same ultrasonic generator, while the grinding machine workbench makes reciprocating motion at velocity v_w and the grinding wheel drives abrasive grains at a speed of v_s in a circular motion. By this process, the 90° 2D ultrasonic-assisted grinding motion is realized, and its kinematic sketch is shown in Fig. 1.

As shown in Fig. 1, the following motions exist under 90° ultrasonic-assisted grinding condition: the grinding wheel demonstrates high-speed rotational motion driven by the principal axis of the grinding machine, the workbench reciprocates rectilinear motion, and the workpiece 2D ultrasonic vibration, as well as the grinding wheel, feed motions in axial and radial directions. The motion of abrasive grains acting upon the workpiece is formed by recombination and superposition of the three motions: rotational motion of the grinding wheel, reciprocating rectilinear motion of the workbench, and ultrasonic vibration of the workpiece.

Elliptic abrasive cutting tracks in Fig. 1 are obtained under reciprocating motion conditions without consideration of grinding wheel rotation, while only relative displacement between abrasive particle and one fixed mass point on the workbench are taken into consideration. This mass point demonstrates simple harmonic vibration along tangential and axial directions simultaneously as driven by the 2D ultrasonic vibration system. According to wave independence principle (also called wave supervision principle), in the encountering space of train waves, the mass point simultaneously participates in the vibration caused by several train waves, and the displacement of the mass point at any time is the vector sum of the displacements under the independent effect of each train wave. For the workpiece in 90° 2D ultrasonic grinding system, one fixed mass point on the workpiece simultaneously

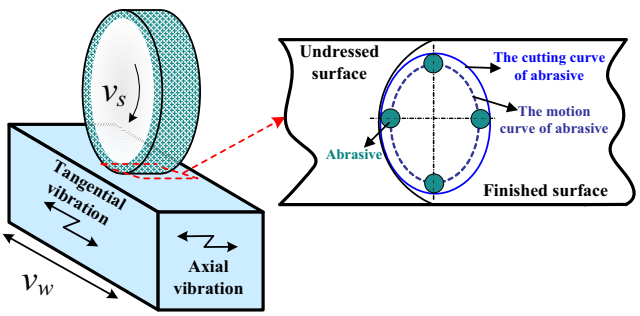

Fig. 1 Kinematic sketch under 90° 2D ultrasonic vibration

participates in simple harmonic vibrations in two mutually perpendicular directions; its displacement is the vector sum of two trains of simple harmonic vibration displacements. The specific conditions are as follows.

During 2D ultrasonic-assisted grinding process, 2D ultrasonic vibrations, which are parallel to and perpendicular to the linear speed direction of the grinding wheel, are applied on the workpiece (Fig. 1), and the trajectory equations of the abrasive grains relative to the workpiece are [16]

$$x = A\cos(2\pi ft) \tag{1}$$

$$y = B\cos(2\pi ft + \varphi) \tag{2}$$

where A is tangential amplitude (μm); B is axial amplitude (μm); f is ultrasonic vibration frequency (Hz); φ is the difference of the initial phase angle between axial and tangential vibrations. Equations 1 and 2 are trajectory equations in which the time parameter t is used to express one mass point on the workpiece surface, and the following formula can be obtained by eliminating parameter t:

$$x^2/A^2 + y^2/B^2 - 2xy\cos\varphi/AB = \sin^2\varphi \tag{3}$$

Formula 3 is an elliptic equation under a rectangular coordinate, namely, the motion trajectory of any mass point on the workpiece. The following can be obtained when the φ value is 90° according to Formula 3:

$$x^2/A^2 + y^2/B^2 = 1 \tag{4}$$

That is to say, the motion trajectory of mass point is an ellipse taking the coordinate axis as the principal axis, and the radii of the short and long axes of the ellipse are decided by A and B. Under the condition in which the phase angle difference value of the ultrasonic generators is 90°, ellipses of different shapes can be obtained by adjusting the angle between the axial ultrasonic vibrator and the tangential ultrasonic vibrator.

If the direction of the tangential ultrasonic vibrator remains unchanged, the angle between axial and tangential ultrasonic vibrators becomes θ. In other words, when θ is less than 90°, the axial ultrasonic vibrator demonstrates $(90-\theta)°$ counterclockwise rotation; while when θ is greater than 90°, the axial ultrasonic vibrator displays $(\theta - 90)°$ clockwise rotation. The vibration equation when the included angle is θ can be obtained according to wave superposition characteristics.

$$\begin{cases} x = A\cos(2\pi ft) - B\sin\theta\cos(2\pi ft + \pi/2) \\ y = B\cos\theta\cos(2\pi ft + \pi/2) \end{cases} \tag{5}$$

Furthermore, Matlab was used to simulate the 2D motion trajectory of the mass point on the workpiece surface within one cycle under 2D ultrasonic vibration from different angles; the specific simulation results are shown in Fig. 2.

As shown in Fig. 2, when the angle between the two ultrasonic vibrators changes, the 2D motion trajectory of the mass point on the workpiece will also change correspondingly. When the included angle of traditional 2D ultrasonic vibration is 90°, the trajectory is as follows: the overlapping length of semi-major axis and axial coordinate of the positive ellipse is 5.5 μm and the overlapping length of semi-minor axis and tangential coordinate is 5 μm. When the included angle changes from 90° to 45° and 135°, the ellipse obviously inclined; and the greater the difference between the included angle and 90°, the larger the oblique cutting angle, contrary to the inclination directions under 45° and 135°. In the meantime, as the inclination angle is enlarged, the semi-major axis is lengthened, while the semi-minor axis is shortened, indicating that vibration has more obvious effect on the tangential direction but correspondingly weakens in the axial direction.

Moreover, based on an analysis of the motion status of one mass point on the workpiece combining the reciprocating motion of the workbench, when the workbench demonstrates a negative motion along the x axis at a speed of 3 m/min, the motion trajectory of one mass point on the workpiece surface is a group of generalized family of spiral surfaces with definite position relationship. This curve can be called "elliptic spiral line." The motion trajectory of elliptic spiral line is of great importance for the formation of a remarkable workpiece surface, and the 45°–135° elliptic spiral line obtained through the simulation is shown in Fig. 3.

3 ZrO_2 ceramic grinding under 2D ultrasonic vibrations

3.1 Experimental conditions

The experiment used a K-p36 grinder (Fig. 4). The main technical parameters of the K-p36 grinder are as follows: 4.5-kW maximum output power of the main grinder spindle and between 45 and 4800 r/min range of spindle speed. The grinder was equipped with a magnetic workbench, and the working range of the magnetic workbench was 600 mm. The size of the magnetic workbench was 950 × 1000 mm. The longitudinal feed velocity of the magnetic workbench was 4–4000 mm/min, and the transverse feed velocity of the magnetic workbench was 30–3000 mm/min. This grinder was equipped with a fixed diamond-head grinding wheel trimmer. A Bluebe MQL feed flow system was adopted. This system applied a pulse generator to regulate the high-precision pumping of MQL oil and compressed air, which can control the flow of feeding lubricant, compressed air, and gas to liquid ratio. The experiment used a 240# CBN grinding wheel with a diameter of 300 mm and a width of 20 mm. The workpiece surface roughness was measured by TIME3220 Surface Profilometer. A S-3500N scanning electron microscope (SEM) was used to conduct surface morphology scanning and energy spectrum analysis.

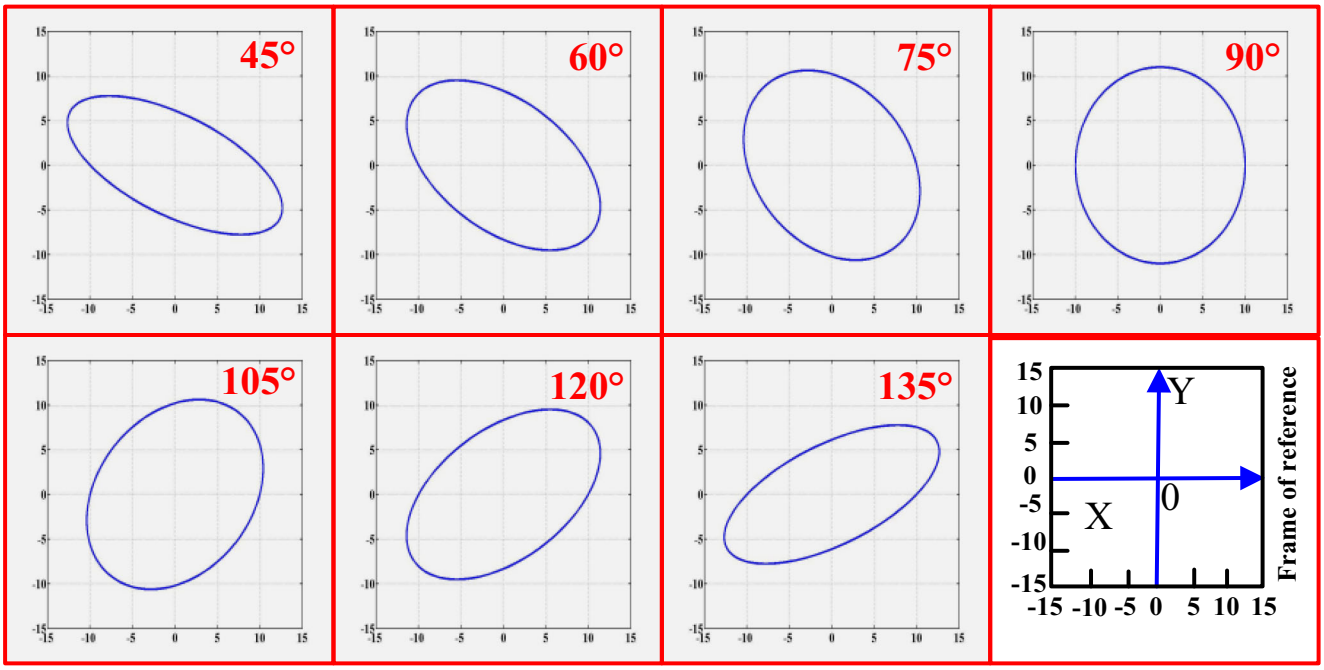

Fig. 2 Motion trajectory under 2D ultrasonic vibration

The frequency range of ultrasonic generators used in the experiment is 19–45 kHz, and the power range is 600–2400 W. The ultrasonic generator generates ultrasonic-frequency electric oscillation signal, which is further transmitted to self-made 2D ultrasonic vibration system. The same-frequency mechanical vibration is generated through an energy converter, and it amplifies the amplitude through an amplitude modulator; and finally, a large enough mechanical vibration amplitude is generated on the workpiece. Self-made 2D ultrasonic vibration system can change the angles of the two ultrasonic vibrators, and the adjustable range of the set angles is within 45°–135° (adjustable every other 15°). Multiangle 2D ultrasonic vibration system can apply variable-angle 2D ultrasonic vibration technology to the grinding process. Different combined vibration directions are generated by regulating the angles of the two ultrasonic vibrators to change the relative motion trajectory of the abrasive grains relative to the workpiece.

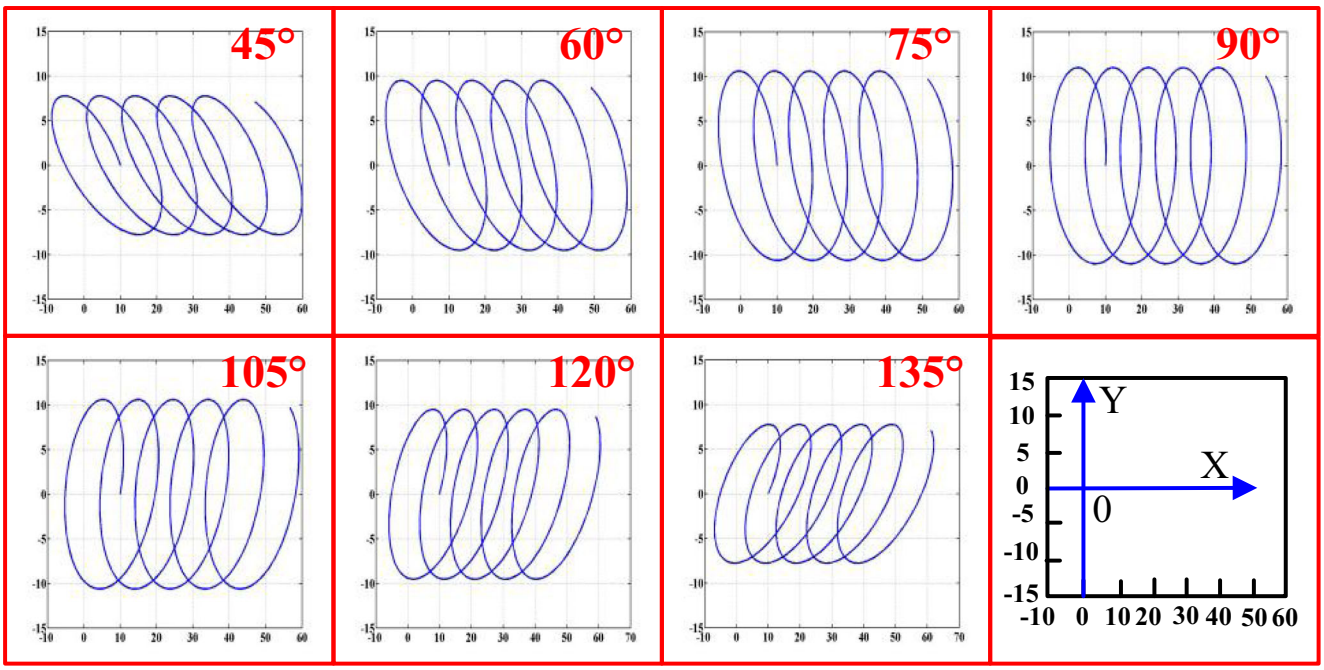

Fig. 3 Elliptic spiral line under different 2D ultrasonic vibrations

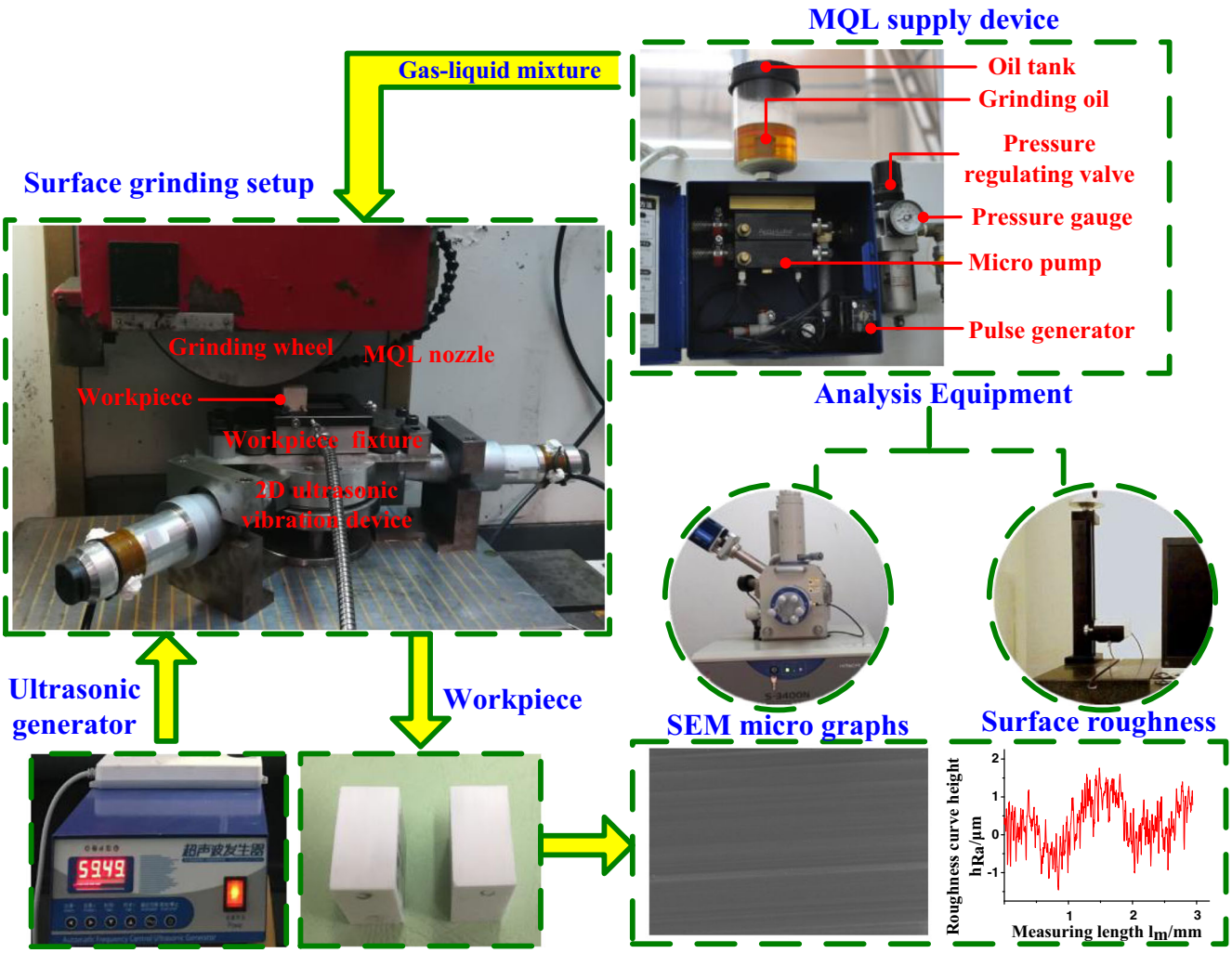

Fig. 4 Experimental setup

Angles of the two-group ultrasonic vibrators used in the experiment are adjustable within 45°–135° (adjustable every other 15°). The frequency and amplitude of the tangential ultrasonic vibrator are 19,960 Hz and 10 μm, respectively; the frequency and amplitude of the axial ultrasonic vibrator are 19,933 Hz and 11 μm, respectively; and the phase difference between the axial ultrasonic vibrator and the tangential ultrasonic vibrator is 90°. The device under the included angles 45° and 135° is seen in Fig. 5.

The material used in the experiment is 3 mol% yttria-stable tetragonal polycrystal zirconia (3 mol% yttrium-stabilized tetragonal zirconium polycrystal, 3Y-TZP); this ZrO_2 is defined as the most extensively applied ceramic material in false tooth. Its mechanical properties are presented in Table 1.

In the machining field, as a biodegradable natural lubricant similar to vegetable oil, palm oil has been extensively applied in green manufacturing [38, 55], and diamond nanoparticles are highly favored by researchers because of their superior heat transfer and lubricating properties. In order to explore into the effects of 2D ultrasonic vibration and the angles of its two vibrators on the surface quality of ZrO_2 ceramic surface grinding under nanofluid MQL condition, diamond nanoparticles with

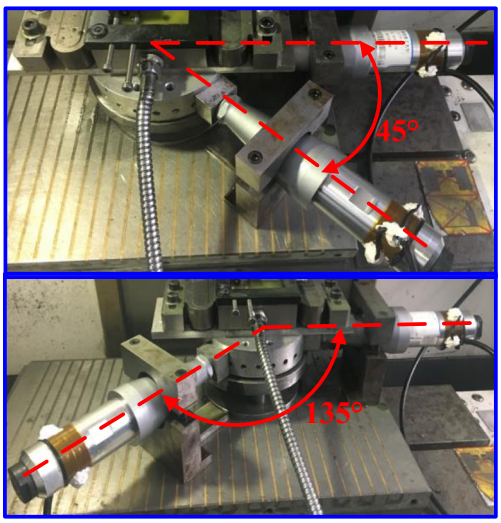

Fig. 5 2D ultrasonic vibration systems of 45° and 135°

Table 1 Mechanical property of 3Y-TZP

Property	Value
Component	3 mol% $Y_2O_3 + ZrO_2$
Crystalline phase	Tetragonal phase
Density (g/cm^3)	6.02
Bending strength (MPa)	800
Compressive strength (MPa)	3000
Elasticity modulus (GPa)	200
Breaking tenacity (MPa·m$^{1/2}$)	8
Microhardness (MPa)	1200
Poisson's ratio	0.3
Thermal expansivity (K^{-1})	10×10^{-6}
Heat conductivity [W/(m·K)]	3

Table 2 Experimental parameters

Grinding parameters	Value
Grinding pattern	Surface grinding
Peripheral speed of grinding wheel v_s (m/s)	30
Feed speed v_w (m/min)	3
Cutting depth a_p (μm)	5
MQL flow rate (ml/h)	60
MQL nozzle distance (mm)	10
MQL nozzle angle (°)	15
MQL gas pressure (bar)	6.0
Vapor-liquid ratio	0.3
Liquid flow rate (kg/s)	0.005
Working environment temperature (°C)	23–25

average particle size of 50 nm were added into the palm oil used in the experiment, and the nanofluid with a volume fraction of 4 vol% was prepared. The nanofluid was prepared by two steps, that is, the prepared nanoparticles are dispersed into the palm oil, and the dispersants are added after sufficient ultrasonic vibration to prevent the agglomeration of the nanoparticles in the palm oil. The mixed surfactants (Span 80 and Polysorbate 80) were prepared according to the volume ratio of 1:1, and the surfactant accounted for 0.3% of the total volume.

In order to investigate the effects of 2D ultrasonic vibration and its different working angles on the surface quality of ZrO_2 ceramic surface grinding, seven groups with different angles (within 45°–135°) of 2D ultrasonic vibration patterns were used in the experiment to implement dry surface grinding. For further studies on the comprehensive influence of nanofluid MQL and 2D ultrasonic vibration combined technique on the finished surface, surface grinding was implemented with the assistance of the seven groups with different angles of 2D ultrasonic vibrations under nanofluid MQL working condition. Ultrasound-free dry surface grinding was used as the reference group in the experiment. After machining, roughness measurement and surface topographical analysis were implemented for the workpiece surface to determine the effects of various working conditions on surface quality. To guarantee accuracy and reliability of the experiment, other machining and jet flow parameters were kept consistent except for the adopted different lubricating modes and ultrasonic vibration angles, specifically as shown in Table 2.

To ensure similar sharpness of the grinding wheel during operation and to acquire a grinding force that is close to the real value, it was trimmed every 100 working steps. The trimming parameters of the grinding wheel are shown in Table 3.

3.2 Result and analysis

First, ultrasound vibration-free dry surface grinding experiment was carried out for ZrO_2 ceramic workpiece. The machined workpiece surface was placed under micromorphology acquisition using SEM, and the results are shown in Fig. 6.

Figure 6a shows the optimal surface acquired under the dry surface grinding condition. Figure 6b–d shows the common feature surface acquired under the dry grinding condition. Under the dry grinding condition, serious material peeling phenomenon occurred on the workpiece surface due to the hard and crisp properties of the ceramic material; and peeling pits were large and deep (Fig. 6b). In the meantime, in view of the serious insufficiency of heat dissipation and cleaning abilities of dry grinding, these debris formed during machining process formed large adhesion points in high-temperature grinding zone, and even enormous adhesion also occurred as shown in Fig. 6c. Under this extremely adverse grinding condition, abrasive grains easily formed deep furrows with rough bottom surface, and lateral materials were seriously accumulated in these furrows with obvious peeling phenomenon (Fig. 6d). Even in the optimal surface acquired under dry grinding condition as shown in Fig. 6a, narrow and deep furrows with rough bottom surface also appeared. With large quantity of debris adhesion, peeling pits, as well as uneven and rough furrows appear on the workpiece surface. The removal of ceramic material was completed through shaping and extension of gaps and cracks. Therefore, the workpiece surface formed under this working condition was not only rough, but the surface and subsurface suffered from serious damage. Moreover, crack propagation caused by uneven stress easily appeared in the workpiece usage, which greatly degraded workpiece use conditions and shortened its service life [56, 57].

Table 3 Parameters of grinding wheel dressing

Dresser type	Fixed PCD dresser of K-P36 grinder
Single stroke trimming amount (mm)	0.01
Transverse feed rate (mm/rev)	0.5
Number of strokes	15

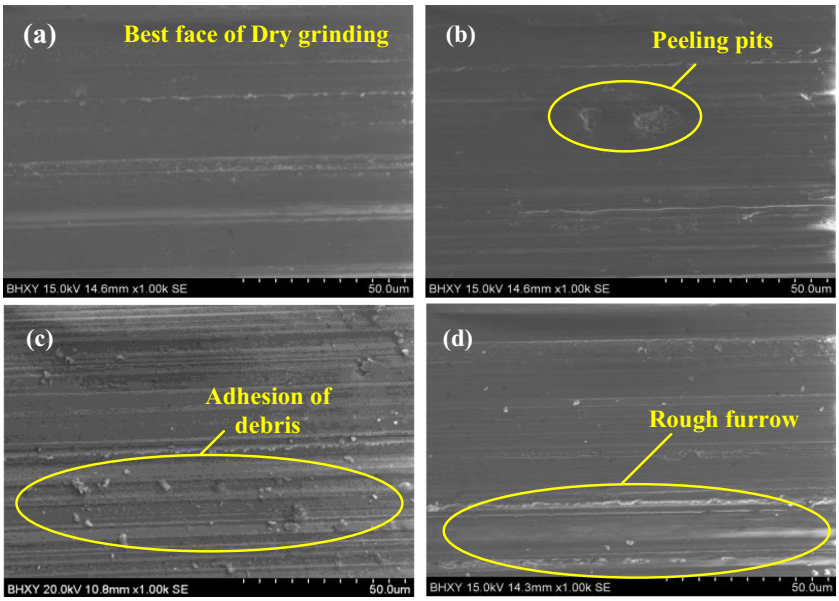

Fig. 6 **a**–**d** Surface topography under conventional dry grinding

2D multiangle axial ultrasonic vibration was added under conventional dry grinding condition in the experiment. The frequency and amplitude of the used tangential ultrasonic vibrator are 19,960 Hz and 10 μm, respectively; the frequency and amplitude of axial ultrasonic vibrator are 19,933 Hz and 11 μm, respectively; and the phase difference of axial and tangential ultrasonic vibrators is 90°. SEM was used to acquire microtopography of the finished workpiece surface as shown in Fig. 7.

Figure 7 shows the surface topographies of ultrasonic-assisted dry grinding surface topography under 45°,60°, 75°, 90°, 105°, 120°, and 135° conditions. After addition of 2D ultrasonic vibration, workpiece surface quality was obviously superior to that under dry grinding without ultrasonic. The adhesion number and size on the workpiece surface was obviously reduced after addition of ultrasonic vibration, and no enormous adhesion was observed compared with that under conventional dry grinding condition. Overall, when the angle is approximately 90° (such as 75° and 105°), adhesion points were larger. In addition, material peeling phenomenon also appeared under 2D ultrasonic vibration, but material peeling zone was obviously smaller and shallower than that under conventional dry grinding. The difference in material peeling phenomenon was not obvious under different angles of ultrasonic vibrations. Compared with workpiece surface under conventional dry grinding, furrows under different angles of ultrasonic vibrations were obviously widened and became shallow; furrow undersurface was relatively smoother; and materials stacked at the two sides of the furrow were flattered with short height.

The abovementioned phenomena that occurred after the addition of 2D ultrasonic vibration were analyzed. Adding 2D ultrasonic vibration on the workpiece contributed to the improvement of workpiece surface quality. Further, the optimization mechanism of ultrasonic vibration for surface quality was concretely analyzed. Without consideration of axial

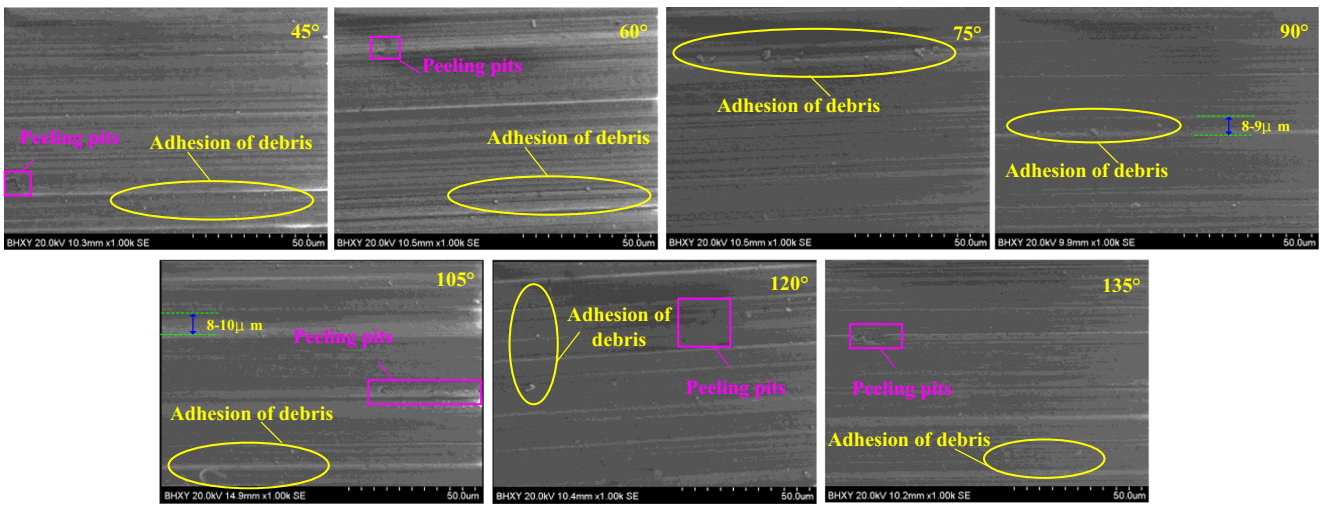

Fig. 7 Surface topography of multiangle ultrasonic-assisted dry grinding

ultrasonic vibration, the tangential motion of one mass point on the workpiece was the vector sum of workbench motion and tangential ultrasonic vibration. The vibration cycle can be obtained (5×10^{-5} s) according to tangential ultrasonic vibration frequency; workbench displacement within one vibration cycle can be obtained (2.5 μm) according to the moving speed of the workbench. Displacements of the workbench and tangential vibration are shown in Fig. 8.

According to Fig. 8, if the initial direction of tangential vibration is consistent with the moving direction of the workbench, the tangential vibration will be in the mode of sinusoidal motion. The displacements of both ultrasonic vibration and workbench are feed displacements at motion starting time t_0. First, the first ultrasonic vibration cycle of one mass point on the workpiece was analyzed. The ultrasonic vibration and workbench motion at motion starting time t_0 made the mass point rapidly move towards the feed direction. If the rotating grinding wheel was regarded as a continuous cutting body, this moment was the starting point of cutting. As ultrasonic vibration displacement rapidly increased, the cutting process continued. At time t_1, the sum of displacements was the maximum feed distance within the first cycle, which is 10.625 μm. Given that back vibration of ultrasonic waves occurred and back vibration speed was higher than the workbench feed speed, this mass point was separated from the grinding wheel. At time t_2, the workbench distance offset vibration was displaced, and this mass point returned to its initial position. Afterwards, the workpiece continued to move away from the grinding wheel under the effect of ultrasonic waves; and at time t_3, the mass point reached the position farthest from the grinding wheel, and the distance was − 0.8.125 μm. After time t_3, ultrasonic vibration changed direction again, and its moving direction was consistent with that of the workbench again. The mass point moved towards the grinding wheel until it contacted the grinding wheel again at time t_4. When the ultrasonic wave is completed, the whole vibration period reaches t_5, the effect of ultrasonic on the displacement of the workpiece is eliminated, and the displacement of the particle is equal to that of the worktable, which is 2.5 μm. The actual machining condition within the first cycle was rapid feed until at the maximum feed displacement of the workpiece. Then, the workpiece demonstrated reverse motion and separated from the grinding wheel. It reached the position farthest from the grinding wheel at time t_3, after which it moved towards the grinding wheel again until it contacted the grinding wheel at the starting point of the grinding process at time t_4. The mass point continued to move towards the feed direction, and the whole vibration cycle was completed at time t_5. This mass point passed the grinding wheel twice. It was located at the stage away from the grinding wheel and then in a follow-up feed stage after completing the first cutting at time t_0.

Even though this mass point went through feed displacement relative to the starting position after completing the first cycle, the workpiece did not reach the maximum cutting position of the first vibration cycle yet at the time. Then, the second ultrasonic vibration cycle started, and the workpiece continued to move forward until the displacement reached the maximum value in the first cycle, after which it started real cutting feed motion to realize workpiece cutting until it reached the maximum cutting displacement position of the second cycle at time t_6. Then, the workpiece was separated from the grinding wheel again. The actual cutting displacement in the second cycle was only 2.5 μm shorter than that in the first cycle, which is consistent with the feed displacement of the workbench in the first vibration cycle. This situation was the similar to that in actual cutting displacements within the third and fourth cycles. Follow-up cyclic motion can be analyzed according to this method until at time t_n in the fourth cycle when this mass point

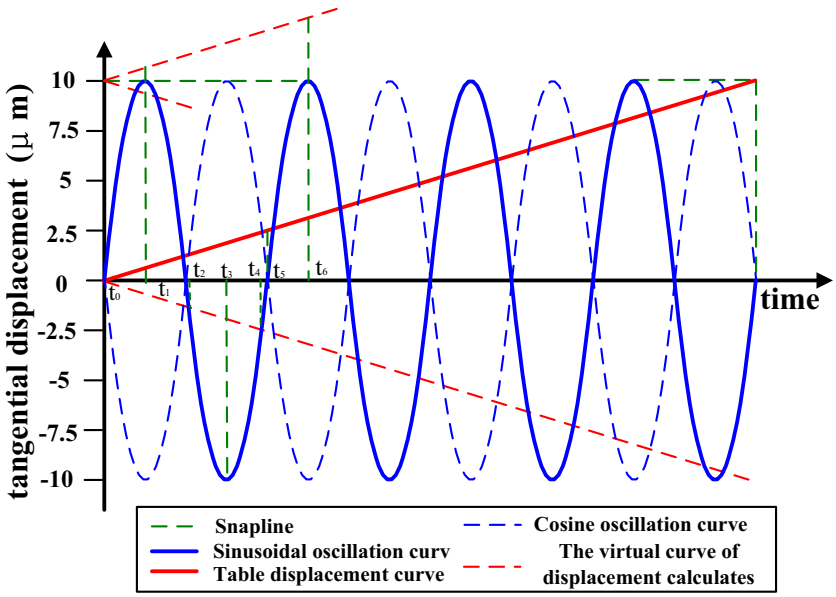

Fig. 8 Displacements of the workbench and tangential vibration

was separated from the grinding wheel. Thus far, this mass point passed the grinding wheel eight times, except for the cutting effect with the grinding wheel at time t_0. To sum up, this mass point completed a cutting process at time t_0, went through buffing effect eight times, and finally did not participate in any cutting motion after radical separation from the grinding wheel. Although the grinding wheel was not a continuous cutting body in actual machining process, multiple buffing and finishing of the mass point on the workpiece can also be realized due to its high rotating speed.

Analysis of this mass point was applicable to all mass points on the workpiece; thus, any mass point on the workpiece experienced one cutting and multiple buffing effects under the effect of tangential ultrasonic vibration, thereby improving the workpiece surface quality. Based on macroscopic analysis, the grinding wheel was under continuous cutting state, and the cutting displacement in each vibration cycle was 2.5 μm. From a microscopic angle, the workpiece and grinding wheel were under a contact-separation-contact-separation cyclic motion. This analytical method can also be used to analyze cosine vibration form and vibration form of any other phase angle.

According to experimental SEM pictures, compared with dry grinding, addition of ultrasonic vibration resulted in widened furrows. Furrow widening was thought to be the product formed under the effects of axial ultrasonic vibration applied on the workpiece. Vibration graphs of the abrasive grains and the workpiece without considering tangential vibration are shown in Fig. 9.

According to Fig. 9, the wheel position was kept unchanged without axial feed motion, and the abrasive particle profile expressed by the imaginary line was the relative position between the workpiece and two abrasive grains before axial ultrasonic vibration. As shown in Fig. 9a, the height and width of nonremoved materials between two abrasive grains when ultrasonic vibration was not added are represented by H and W, respectively. After addition of axial ultrasonic vibration, the workpiece experienced axial displacement under the effect of ultrasonic vibration. Figure 9b, c demonstrates relative positions when axial ultrasonic waves vibrate leftward and rightward towards the maximum amplitude B. When the workpiece vibrated leftward towards the maximum amplitude under the effect of ultrasonic waves, the left-side abrasive particle further cut the residual material between the two abrasive grains. After cutting, the height and width of the nonremoved material are represented by H' and W', respectively. Afterwards, when the workpiece vibrated rightward towards the maximum amplitude, the right-side abrasive particle cut the residual material between the two abrasive grains again, and the height and width of the nonremoved material are represented by H'' and W'', respectively, after cutting.

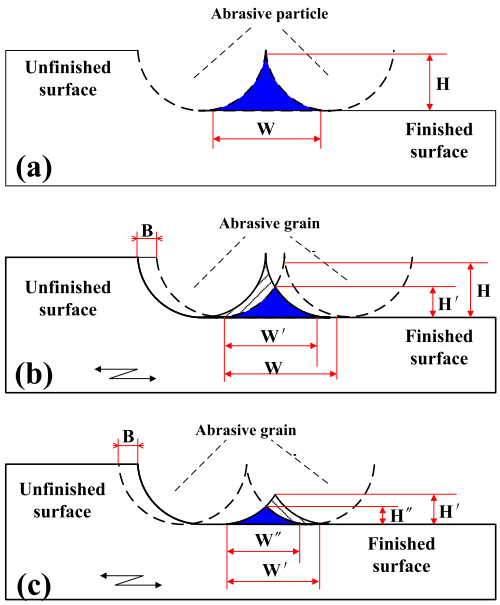

Fig. 9 **a**–**c** Vibration graphs of the abrasive grains and workpiece under axial ultrasonic vibration

The effect of axial ultrasonic vibration on the motion trajectory of abrasive grain was mainly manifested at furrow width on the workpiece surface. The larger the axial ultrasonic vibration amplitude B, the wider the furrow on the workpiece surface. If one abrasive particle is always at a plowing state within one axial vibration cycle, then the maximum width of furrows on the workpiece surface can increase to $2B$. However, according to experimental parameters, the abrasive grains have already been separated from the cutting process when one vibration circle was not yet completed; thus, the width of furrows will not reach the maximum value. Reflecting axial vibration cutting trajectory on numerous abrasive grains, the interference degree between abrasive grains would be greatly strengthened so that uncut materials on the grinding surface would be obviously reduced in both width and height to effectively improve grinding surface quality.

Based on the above analysis of tangential and axial ultrasonic-assisted grinding mechanism, compared with conventional grinding, 2D ultrasonic-assisted grinding process exhibited more “one-time cutting and multi-buffing” and “furrow shoaling and widening” effects to obtain more ideal workpiece surface quality. Given that no lubricating and cooling media participated in this working condition, the grinding zone cannot be sufficiently cooled and lubricated; therefore, adhesion points still appeared on the workpiece surface. However, compared with dry grinding, both the quantity of size of adhesion points were obviously reduced. Through a comparison of 2D ultrasonic surfaces under different angles, the closer the angle was to 90°, the wider the furrows. Furthermore, the unevenness of the furrow undersurface was intensified, and the size of adhesion points slightly enlarged. According to analysis, when the angle was close to 90°, the axial effect of 2D ultrasonic vibration was enhanced but the tangential effect was degraded.

In order to further discuss the influence of 2D ultrasonic vibration on the workpiece surface under lubricating condition, nanofluid MQL 2D ultrasonic vibration test was imple

mented, and zirconia ceramic surface grinding experiment was carried out under different angles of 2D ultrasonic vibrations. The nanofluid parameters used in the experiment were similar to the abovementioned. SEM was used to acquire the microtopography of the finished workpiece surface as shown in Fig. 10.

Figure 10 shows the surface topography of ultrasonic-assisted nanofluid MQL grinding under 45°, 60°, 75°, 90°, 105°, 120°, and 135° conditions. After addition of nanofluid lubrication based on 2D ultrasonic vibration, workpiece surface quality was obviously improved. Adhesion phenomenon on workpiece surface was obviously reduced after addition of nanofluid lubrication, and some adhesion phenomena on the surface basically disappeared. Moreover, material peeling phenomenon was also greatly improved, and material peeling zones were obviously reduced, which were also shallower and smaller than those under the nonlubricating condition. Overall, after addition of nanofluid lubrication, workpiece surface quality was obviously improved, and the quantities, as well as the sizes, of adhesion points and material peeling regions were obviously reduced.

Furthermore, based on the analysis of the improvement of workpiece surface quality after addition of NMQL, nanofluid addition provided relatively ideal cooling and lubricating effect for the grinding zone [58–60]. In addition, according to the analysis of the combined ultrasonic vibration, ultrasonic-assisted grinding would more easily result in the appearance of microchannel in the grinding zone. This microchannel can improve the cooling and heat transfer performances of MQL and nanoparticles. Under conventional dry grinding condition, abrasive grains closely contacted the two sides of the furrow after cutting into the workpiece and even adhesion phenomenon between the side faces of abrasive grains and workpiece material occurred. After addition of 2D ultrasonic vibration, furrows were widened; and gaps appeared at the edges of abrasive grains and furrows to form microchannels, which provided more ideal conditions for the entrance of MQL, specifically as shown in Fig. 11.

As shown in Fig. 11, abrasive grains widened the furrows after the addition of ultrasonic waves. Compared with conventional dry condition, the furrows could be widened by a width of b with the help of ultrasonic waves, and the stacking materials at the edge of the furrows will not directly contact abrasive grains, thus forming microchannels. Under no ultrasonic effect, MQL can form directional transportation towards the debris on the workpiece surface and side-face regions of abrasive grains only by relying on aerodynamic force provided by compressed air. At the time, abrasive grains contact debris; thus, entry between abrasive grains and debris difficult for the nanofluid; the lubricating film cannot form abrasive/rake face and workpiece/flank face, and even a small quantity of lubricant infiltration cannot ensure lubrication between rake face and debris. However, furrows were widened after addition of ultrasonic vibration; microchannels were formed at the side walls of furrows and between abrasive grains. The existence of these microchannels provided necessary spaces for the transportation of nanofluid towards rake face. Moreover, the separation stage between workpiece and abrasive grains would occur under the effect of tangential ultrasonic vibration, during which, a small storage space appeared in the abrasive grains and non-machined region; while the lubricant would be stored in this space after passing the microchannels. When the abrasive grains contacted with the workpiece again, the lubricating film can provide lubrication between abrasive/rake face and workpiece/flank face. During forward transportation process of nanofluid through microchannels, oil films would also be formed at the microchannel bottom and side walls. The formed lubricating oil films would exert lubricating effect during multiple finishing processes of furrow bottom surface and furrow side faces, which further improved the smoothness of furrow bottom surface and side walls and helped obtain more ideal workpiece surface.

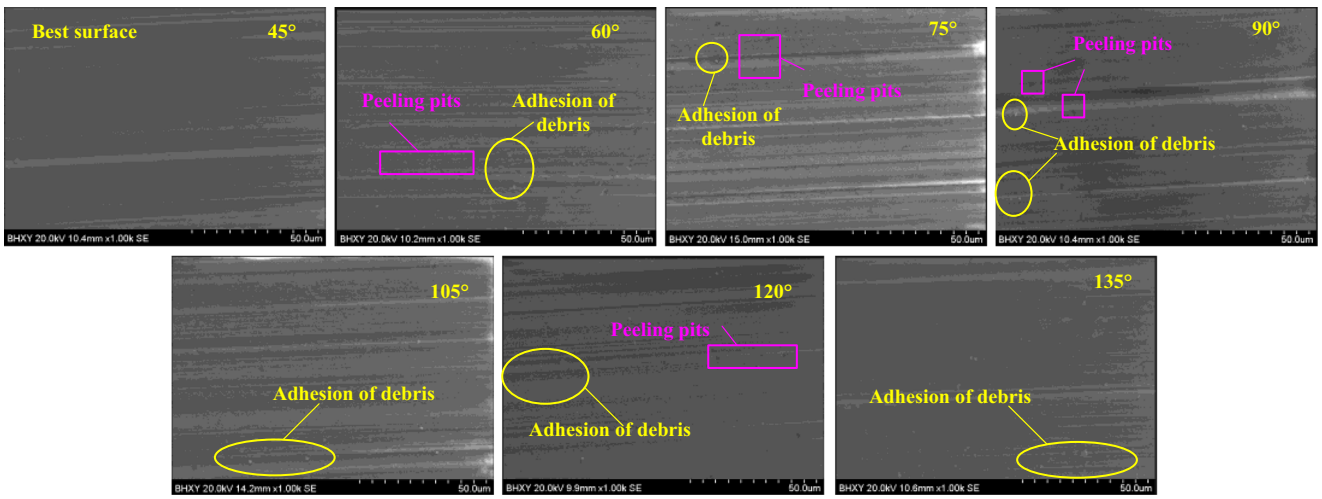

Fig. 10 Surface topography under the simultaneous utilization of 2D UAG grinding and NMQL

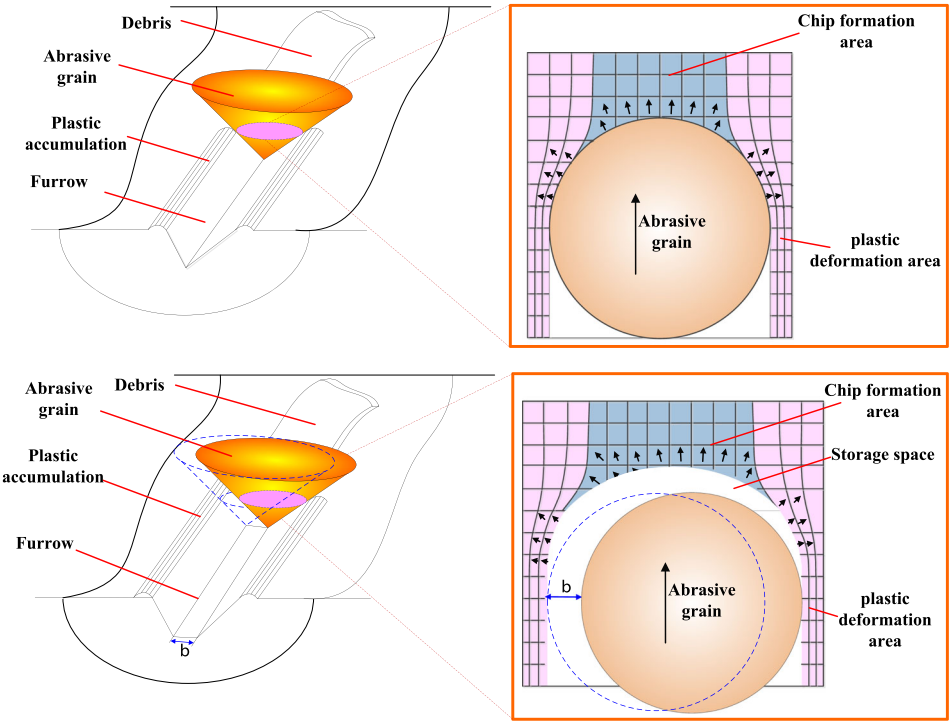

Fig. 11 Formation of microchannel by 2D UAG

Moreover, scattered nanoparticles in nanofluid constituted internal structural defect of lubricating oil. Given that nanoparticles had small particle sizes and thermal motion played a significant role, they can be considered as moving structural defects in lubricants; and these defects can also be called cavitation nuclei. Existence of cavitation nuclei and external ultrasonic vibration constituted two necessary conditions for cavitation effect. Cavitation effect would be formed in nanofluid under the effect of ultrasonic waves to generate a large quantity of cavitation bubbles. These cavitation bubbles would experience drastic oscillation and even collapse under the effects of ultrasonic vibration and self-disturbance of grinding process. Bubbles presented sharp linear change when cavitation bubbles collapsed, which would release high-speed microjet with intense impact waves. The generated instantaneous local high temperature can reach 10^2–10^4 K, and local high pressure can reach 10^{-3}–10^4 MPa [61]. Impact waves would generate intense impact on the surrounding lubricant, workpiece, and workpiece/abrasive particle interface. The impact would drive the lubricant to permeate around and enter the oil storage region through the microchannel. This was helpful to draw into film on the workpiece surface. When the impact acted upon workpiece interface, burrs and small adhesion points on the workpiece surface can be removed, which can help to further improve surface quality. When the impact acted upon abrasive grains, abrasive grains would break to form a new cutting edge, which helped maintain the sharpness of abrasive grains and improve follow-up cutting performance. In addition, ultrasonic wave impact can drive diamond nanoparticles to move at a high speed. The diamond would exert a polishing effect on the workpiece surface due to its extremely high hardness to improve workpiece surface smoothness.

According to Fig. 10, when the included angle between axial and tangential ultrasonic vibrators goes further away (larger or smaller) from 90°, the workpiece surface quality was more ideal. Based on analysis, under multiangle 2D ultrasonic-assisted grinding condition, the relative motion of abrasive grains on the grinding wheel and workpiece surface formed microchannels with different morphologies exhibited pumping effects on the lubricant to different degrees. The greater the ratio of tangential to axial microchannels, the stronger the pumping effect, because the greater the ratio, the longer and thinner the formed microchannels and the stronger the axial flow conductivity of the nanofluid. Through the above analysis of abrasive particle path, the tangential to axial ratios of microchannels under 45° and 135° were the greatest. On the other hand, when the included angle θ of two ultrasonic vibrators was from 45° to 135°, the tangential effect of ultrasonic vibration was more obvious. After vector superposition, the enlargement of tangential amplitude and reduction of axial amplitude at the time were the most obvious; thus, a larger storage space would be formed in the abrasive grains and nonmachined region during the separation process of abrasive grains from the workpiece. This effect was good for more nanofluids to enter, which will provide more ideal conditions for subsequent lubrication. In addition, when the included angle between two ultrasonic vibrators was 90°, as the geometrical shape of microchannels presented circumferential symmetry concerning the circular velocity of the grinding wheel without directional effect which made the lubricant

move, nearly no pumping effect was observed, and nanofluid infiltration effect was poor. When the included angle was 45° and 135°, the pumping effect was the strongest [62, 63], and at the time, the microchannel exhibited intense guiding effect on nanofluid flow. A large quantity of nanofluid was pumped into the storage space to obtain favorable lubricating effect.

Furthermore, workpiece surface roughness *R*a and *RSm* values in vertical grinding direction under conventional dry grinding, ultrasonic-assisted dry grinding, and ultrasonic vibration NMQL conditions were measured. The surface roughness *R*a values along the grinding direction under conventional dry grinding and ultrasonic-assisted dry grinding conditions were measured. Figure 12 shows the measured values under conventional dry grinding and different angles of ultrasonic-assisted dry grinding conditions.

As shown in Fig. 12, maximum roughness *R*a value (0.972 μm) was obtained under conventional dry grinding condition. The *R*a value was obviously reduced after addition of 2D ultrasonic vibration. As the angle increased, the *R*a value presents an increasing trend first followed by decreasing trend. The *R*a value obtained a minimum value of 0.73 μm when the tangential and axial included angle was 45°. When the angle is increased to 90°, the maximum *R*a value (0.86 4 μm) was obtained under ultrasonic-assisted dry grinding condition. Minimum *RS*m value (0.068 mm) was obtained under conventional grinding condition. Similarly, as the angle increased, the *RS*m value presents an increasing trend first and then decreases. The *RS*m value obtained the maximum value of 0.089 μm when the tangential and axial included angle was 90°. When the angle is increased to 135°, the minimum *RS*m value (0.071 μm) was obtained under ultrasonic-assisted dry grinding condition. We believe that furrows presented widening and shoaling features under the effect of axial ultrasonic vibration. Moreover, multiple finishing effects of tangential ultrasonic vibration also improved smoothness.

Surface roughness *R*a values (error bars represent standard deviation in data) along the grinding direction, namely, longitudinal direction of furrows under conventional dry grinding and ultrasonic-assisted dry grinding conditions, were measured as shown in Fig. 13.

The roughness values of the workpiece surfaces along the grinding direction were measured to characterize the roughness of furrow bottom surfaces. As shown in Fig. 13, furrow bottom surfaces were the roughest under conventional dry grinding condition, and the *R*a value reached as high as 0.131 μm. After addition of 2D ultrasonic vibration, the roughness *R*a value obviously reduced. When the included angle between tangential and axial ultrasonic vibrator was 90°, the maximum *R*a value (0.072 μm) was obtained. As the included angle increased beyond 90°, the *R*a value continuously reduced. Minimum *R*a value (0.037 μm) was obtained when the included angle was 45°. Based on analysis, the abrasive grain exhibited multiple finishing effects on furrow bottom surface under the effect of tangential ultrasonic vibration, which greatly reduced roughness of furrow bottom surface. When the included angle between ultrasonic vibrators was reduced or enlarged from 90°, axial ultrasonic vibrator formed a component in tangential direction, which had the effect of enhancing tangential ultrasonic vibration; thus, the roughness value of furrow bottom surface was further reduced.

NMQL was further added based on 2D ultrasonic vibration, and the *R*a and *RS*m values of workpiece surface roughness were obtained as shown in Fig. 14.

As shown in Fig. 14, the surface qualities under the simultaneous utilization of 2D UAG grinding and NMQL conditions were obviously better than that under nonlubricating condition. As the angle increased, *R*a and *RS*m values also increased first and then decreased. Maximum *R*a and *RS*m values were obtained (0.703 μm and 0.106 mm, respectively) at 90°, and minimum *R*a value (0.585 μm) was obtained under

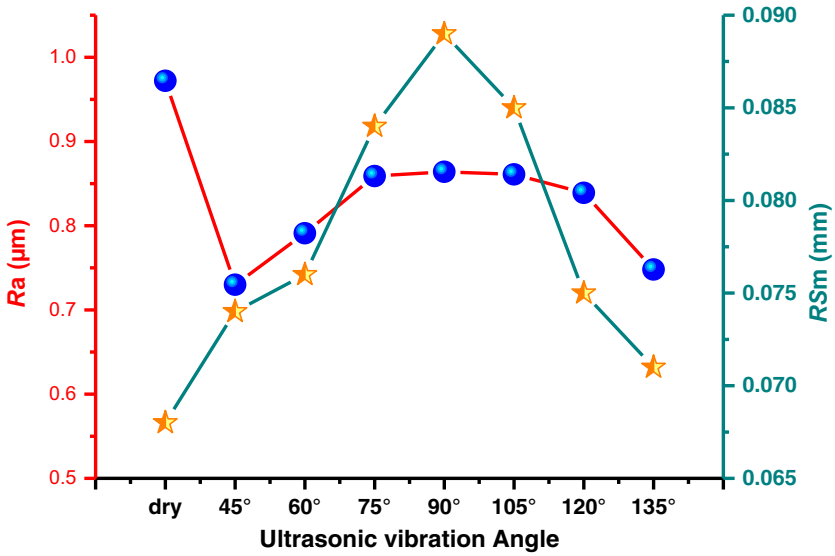

Fig. 12 Roughness values under conventional dry grinding and 2D UAG dry grinding

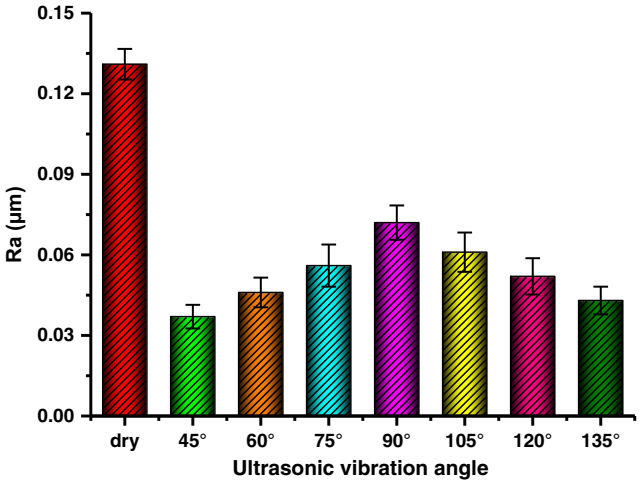

Fig. 13 Roughness along the grinding direction under conventional dry grinding and 2D UAG dry grinding

45°. The minimum *RS*m value (0.76 mm) was obtained under 135°. The *RS*m value under the simultaneous utilization of 2D UAG grinding and NMQL increased slightly compared with that under ultrasonic-assisted dry grinding, possibly because cavitation impact and nanoparticle polishing effect were generated after addition of NMQL and the generated furrows were further widened. Compared with nonlubricating condition, the *R*a value decreased obviously after addition of nanofluid; thus, the nanofluid provided ideal lubricating effect for the grinding zone. In addition, the most ideal effect was observed at under 45° and 135° conditions. We believe that the microchannel flow conductivity was the most ideal at the time, and more nanofluid can enter into the grinding zone to provide sufficient lubricating effect for the rake face and flank face of abrasive grain. Changing the included angle between 2D ultrasonic vibrators helped improve the lubrication effect of nanofluid and improve the workpiece surface quality.

4 Conclusion

Multiangle 2D ultrasonic vibration was utilized and compared with dry grinding in zirconia ceramics grinding. Furthermore, the synergistic effect of multiangle 2D ultrasonic and NMQL was studied. Conclusions can be drawn on experimental basis as follows.

(1) The maximum *R*a value (0.972 μm) and minimum *RS*m value (0.068 mm) were recorded in dry grinding. When 2D ultrasonic vibration is added, the *R*a value decreased significantly, and the *RS*m value demonstrated an opposite trend. As the angle increased, the roughness value (*R*a and *RS*m) presented first an increasing tend and then decreased. The minimum *R*a value (0.585 μm) was obtained under 45°, and the largest *RS*m value (0.089 mm) was obtained under 90°.

(2) When 2D ultrasonic vibration is added, the adhesion and peeling on workpiece surface are obviously reduced compared with dry grinding without ultrasonic vibration. Nevertheless, the distinction of workpiece surface between different angles is not obvious. In addition, the furrows under 2D ultrasonic vibrations are wider and shallower compared with dry grinding, and the undersurface is relatively smoother. The ideal surface is obtained by the "one-time cutting and multi-buffing" and "furrow shoaling and widening" effects of 2D ultrasonic vibration.

(3) Surface qualities under multiangle 2D ultrasonic vibration with NMQL conditions were obviously better than the conditions without lubrication. Similarly, as the angle increased, the roughness value (*R*a and *RS*m) presented an increasing trend first and then decreased. The maximum *R*a and *RS*m values were obtained (0.703 μm and 0.106 mm, respectively) at 90°, and the minimum *R*a

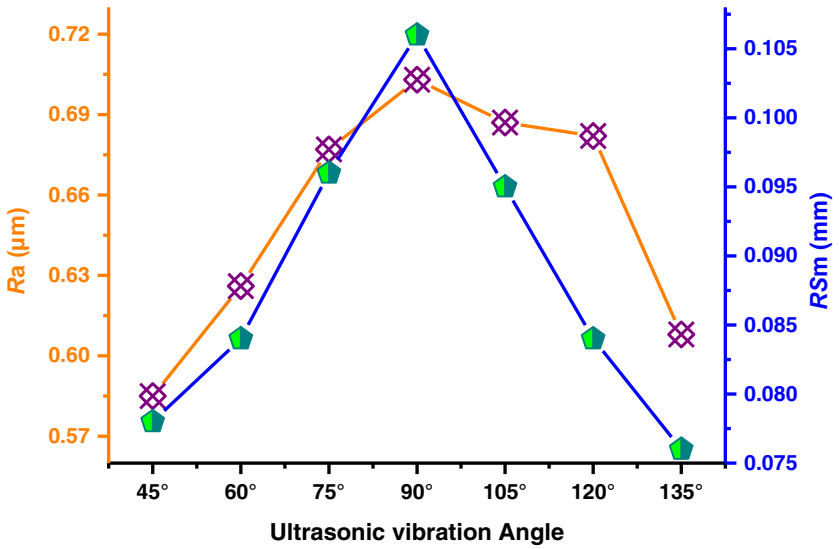

Fig. 14 Roughness values versus angles under the simultaneous utilization of 2D UAG grinding and NMQL

value (0.585 μm) was obtained under 45°. The least *RS*m value (0.76 mm) was obtained under 135°.

(4) The surface quality was further improved by the simultaneous utilization of NMQL lubrication and 2D ultrasonic vibration. The phenomenon of adhesion decreased sharply and even disappeared on some surfaces. In addition, material peeling was also further improved: material peeling area is significantly reduced and the depth was shallower than the nonlubricated conditions. Therefore, 2D ultraso nic-assisted grinding would result in microchannel in the grinding zone between the workpiece and the abrasive grain. Moreover, the permeability and lubrication performance of the nanofluids were enhanced under the combined action of cavitation and pumping function.

Funding information This research was financially supported by the following foundations: the National Natural Science Foundation of China (51575290), Major Research Project of Shandong Province (2017G GX30135 and 2018GGX103044), and Shandong Provincial Natural Science Foundation, China (ZR2017PEE002 and ZR2017PEE011).

References

1. Yang M, Li C, Zhang YB, Jia DZ, Zhang XP, Hou YL, Li RZ, Wang J (2017) Maximum undeformed equivalent chip thickness for ductile-brittle transition of zirconia ceramics under different lubrication conditions. Int J Mach Tools Manuf 122:55–65
2. Ding WF, Dai CW, Yu TY, Xu JH, Fu YC (2017) Grinding performance of textured monolayer cbn wheels: undeformed chip thickness nonuniformity modeling and ground surface topography prediction. Int J Mach Tools Manuf 122:66–80
3. Zhao B, Tianyu YU, Ding WF, Li XY (2017) Effects of pore structure and distribution on strength of porous Cu-Sn-Ti alumina composites. Chin J Aeronaut 30(6):2004–2015
4. Liu CJ, Ding WF, Yu TY, Yang CY (2017) Materials removal mechanism in high-speed grinding of particulate reinforced titanium matrix composites. Precis Eng 51:68–77
5. Qian N, Ding WF, Zhu YJ (2018) Comparative investigation on grindability of k4125 and inconel718 nickel-based superalloys. Int J Adv Manuf Technol 97:1649–1661
6. Xi XX, Yu TY, Ding WF, Xu JH (2018) Grinding of Ti 2 ALNb intermetallics using silicon carbide and alumina abrasive wheels: tool surface topology effect on grinding force and ground surface quality. Precis Eng 53:134–145
7. Zhu ZW, To S, Xiao GB, Ehmann KF, Zhang GQ (2016) Rotary spatial vibration-assisted diamond cutting of brittle materials. Precis Eng 44:211–219
8. Tawakoli T, Azarhoushang B (2008) Influence of ultrasonic vibrations on dry grinding of soft steel. Int J Mach Tools Manuf 48(14): 1585–1591
9. Li KM, Hu YM, Yang ZY, Chen MY (2012) Experimental study on vibration-assisted grinding. J Manuf Sci Eng 134(4):041009
10. Zheng SY, Feng PF, Xu XP (2009) Development trends of rotary ultrasonic machining technology. J Tsinghua Univ 49(11):1799–1804
11. Zheng W, Zhou M, Zhou L (2017) Influence of process parameters on surface topography in ultrasonic vibration- assisted end grinding of SiCp/Al composites. Int J Adv Manuf Technol 91(5):1–12
12. Chen ZY, Wu Y, Yang Y, Li JP, Xie BS, Li XJ, Lei S, Ou-Yang J, Yang XF, Zhou QF, Zhu BP (2018) Multilayered carbon nanotube yarn based optoacoustic transducer with high energy conversion efficiency for ultrasound application. Nano Energy 46:314–321
13. Ni CB, Zhu LD, Liu CF, Yang ZC (2018) Analytical modeling of tool-workpiece contact rate and experimental study in ultrasonic vibration-assisted milling of ti–6al–4v. Int J Mech Sci 142-143:97–111
14. Sun C, Niu YJ, Liu ZX, Wang YS, Xiu SC (2017) Study on the surface topography considering grinding chatter based on dynamics and reliability. Int J Adv Manuf Technol 92(9–12):1–14
15. Liang Z, Wang X, Wu Y, Xie L, Liu Z, Zhao W (2012) An investigation on wear mechanism of resin-bonded diamond wheel in elliptical ultrasonic assisted grinding (EUAG) of monocrystal sapphire. J Mater Process Technol 212(4):868–876
16. Yan YY, Zhao B, Liu J (2009) Ultraprecision surface finishing of nano-zro_2, ceramics using two-dimensional ultrasonic assisted grinding. Int J Adv Manuf Technol 43(5–6):462–467
17. Tian M, Liang ZQ, Wang QY, Wang XB, Zhou TF, Wu YG, Jiao L (2016) Effect of single grit impacts on initiation and propagation condition of cracks in ultrasonic assisted grinding of ceramics by using SPH method. J Mech Eng 16th Int Man Conf China 625–630
18. Zhou M, Huang C, Zhao PY, Huang S (2017) Experimental investigation on subsurface damages in ultrasonic assisted grinding of optical glass. Tool Eng 51(7):15–19
19. Zhang J, Zhao Y, Zhang S, Tian F, Guo L, Dai R (2014) Study on effect of ultrasonic vibration on grinding force and surface quality in ultrasonic assisted micro end grinding of silica glass. Shock Vib 2014(2):1–10
20. Liu LF, Zhang FH, Liu MH (2015) Ultrasonic assisted grinding for silicon carbide. Opt Precis Eng 23(8):2229–2235
21. Ding K, Fu YC, Su HH, He T, Yu XZ, Ding GZ (2014) Experimental study on ultrasonic assisted grinding of C/SiC composites. Key Eng Mater 620:128–133
22. Li C, Zhang F, Meng B, Liu L, Rao X (2016) Material removal mechanism and grinding force modelling of ultrasonic vibration assisted grinding for SiC ceramics. Ceram Int 43(3)
23. Nik MG, Movahhedy MR, Akbari J (2012) Ultrasonic-assisted grinding of Ti6Al4 V alloy. Procedia Cirp 1(1):353–358
24. Tawakoli T, Azarhoushang B, Rabiey M (2009) Ultrasonic assisted dry grinding of 42CrMo4. Int J Adv Manuf Technol 42(9–10):883–891
25. Isobe H, Hara K, Kyusojin A, Okada M (2007) Yoshihara H. ultrasonically assisted grinding for Mirror surface finishing of dies with electroplated diamond tools. Precis Eng 8(2):38–43
26. Abdullah A, Farhadi A, Pak A (2012) Ultrasonic-assisted dry creep-feed up-grinding of superalloy Inconel738LC. Exp Mech 52(7):843–853
27. Nomura M, Wu YB, Kuriyagawa T, Kawashima T, Shibata T (2009) Effects of grain size and concentration of grinding wheel in ultrasonically assisted grinding. Key Eng Mater 389-390:283–288
28. Mahaddalkar PM, Miller MH (2014) Force and thermal effects in vibration-assisted grinding. Int J Adv Manuf Technol 71(5–8):1117–1122
29. Zhang DK, Li CH, Zhang YB, Zhou DZ, Zhang XW (2015) Experimental research on the energy ratio coefficient and specific grinding energy in nanoparticle jet MQL grinding. Int J Adv Manuf Technol 78:1275–1288
30. Rahmati B, Sarhan AAD, Sayuti M (2014) Investigating the optimum molybdenum disulfide (MoS2) nanolubrication parameters in CNC milling of AL6061-T6 alloy. Int J Adv Manuf Technol 70:1143–1155
31. Mao C, Zou HF, Huang XM, Zhang JA, Zhou ZX (2013) The influence of spraying parameters on grinding performance for nanofluids minimum quantity lubrication. Int J Adv Manuf Technol 64:1791–1799
32. Okada M, Hosokawa A, Asakawa N, Ueda T (2014) End milling of stainless steel and titanium alloy in an oil mist environment. Int J Adv Manuf Technol 74:1255–1266

33. Boswell B, Islam MN, Davies IJ, Ginting YR, Ong AK (2017) A review identifying the effectiveness of minimum quantity lubrication (MQL) during conventional machining. Int J Adv Manuf Technol 92:321–340
34. Oliveira GDP, Fonseca MC, Araujo AC (2017) Analysis of residual stress and cutting force in end milling of Inconel 718 using conventional flood cooling and minimum quantity lubrication. Int J Adv Manuf Technol 92:3265–3272
35. Mia M, Bashir MA, Khan MA, Dhar NR (2017) Optimization of MQL flow rate for minimum cutting force and surface roughness in end milling of hardened steel (HRC 40). Int J Adv Manuf Technol 89:675–690
36. Li BK, Li CH, Zhang YB, Wang YG, Jia DZ, Zhang NQ, Wu QD, Ding WF (2017) Numerical and experimental research on the grinding temperature of minimum quantity lubrication cooling of different workpiece materials using vegetable oil-based nanofluids. Int J Adv Manuf Technol 93(5–8):1971–1988
37. Li BK, Li CH, Zhang YB, Wang YG, Jia DZ, Yang M, Zhang NQ, Wu QD, Han ZG, Sun K (2017) Heat transfer performance of MQL grinding with different nanofluids for Ni-based alloys using vegetable oil. J Clean Prod 154:1–11
38. Wang YG, Li CH, Zhang YB, Li BK, Yang M, Zhang XP, Guo SM, Liu GT (2016) Experimental evaluation of the lubrication properties of the wheel/workpiece interface in MQL grinding with different nanofluids. Tribol Int 99:198–210
39. Kalita P, Malshe AP, Kumar SA, Yoganath VG, Gurumurthy T (2012) Study of specific energy and friction coefficient in minimum quantity lubrication grinding using oil-based nanolubricants. J Manuf Process 14(2):160–166
40. Lee PH, Nam TS, Li C, Sang WL (2011) Environmentally-friendly nano-fluid minimum quantity lubrication (MQL) meso-scale grinding process using nano-diamond particles. ICMA Int Conf IEEE 44–49
41. Mao C, Zou H, Huang X, Zhou Z (2012) Investigation of grinding characteristic using nanofluid minimum quantity lubrication. Int J Precis Eng Manuf 13(10):1745–1752
42. Shen B, Shih AJ, Tung SC (2008) Application of nanofluids in minimum quantity lubrication grinding. Tribol Trans 51(6):730–737
43. Zhang YB, Li CH, Yang M, Jia DZ, Wang YG, Li BK, Hou YL, Zhang NQ, Wu QD (2016) Experimental evaluation of cooling performance by friction coefficient and specific friction energy in nanofluid minimum quantity lubrication grinding with different types of vegetable oil. J Clean Prod 139:685–705
44. Zhang YB, Li CH, Jia DZ, Zhang DK, Zhang XW (2015) Experimental evaluation of MoS2 nanoparticles in jet MQL grinding with different types of vegetable oil as base oil. J Clean Prod 87:930–940
45. Zhang YB, Li CH, Jia DZ, Li BK, Wang YG, Yang M, Hou YL, Zhang XW (2016) Experimental study on the effect of nanoparticle concentration on the lubricating property of nanofluids for MQL grinding of Ni-based alloy. J Mater Process Technol 232:100–115
46. Zhang YB, Li CH, Jia DZ, Zhang DK, Zhang XW (2015) Experimental evaluation of the lubrication performance of MoS 2/CNT nanofluid for minimal quantity lubrication in Ni-based alloy grinding. Int J Mach Tools Manuf 99:19–33
47. Zhang YB, Li CH, Ji HJ, Yang XH, Yang M, Jia DZ, Zhang XP, Li RZ, Wang J (2017) Analysis of grinding mechanics and improved predictive force model based on material-removal and plastic-stacking mechanisms. Int J Mach Tools Manuf 122:81–97
48. Yang M, Li CH, Zhang YB, Wang YG, Li BK, Jia DZ, Hou YL, Li RZ (2017) Research on microscale skull grinding temperature field under different cooling conditions. Appl Therm Eng 126:525–537
49. Yang M, Li CH, Zhang YB, Wang YG, Li BK, Hou YL (2017) Experimental research on microscale grinding temperature under different nanoparticle jet minimum quantity cooling. Mater Manuf Process 32:589–597
50. Yang M, Li CH, Zhang YB, Jia DZ, Zhang XP, Hou YL, Shen B, Li RZ (2017) Microscale bone grinding temperature by dynamic heat flux in nanoparticle jet mist cooling with different particle sizes. Mater Manuf Process 6:1–11
51. Jia DZ, Li CH, Zhang DK, Zhang YB, Zhang XW (2014) Experimental verification of nanoparticle jet minimum quantity lubrication effectiveness in grinding. J Nanopart Res 16:1–15
52. Jia DZ, Li CH, Zhang YB, Yang M, Wang YG, Guo SM, Cao HJ (2017) Specific energy and surface roughness of minimum quantity lubrication grinding Ni-based alloy with mixed vegetable oil-based Nanofluids. Precis Eng 50:248–262
53. Jia DZ, Li CH, Zhang YB, Zhang DK, Zhang XW (2016) Experimental research on the influence of the jet parameters of minimum quantity lubrication on the lubricating property of Ni-based alloy grinding. Int J Adv Manuf Technol 82(1–4):617–630
54. Molaie MM, Akbari J, Movahhedy MR (2016) Ultrasonic assisted grinding process with minimum quantity lubrication using oil-based nanofluids. J Clean Prod 129:212–222
55. Guo SM, Li CH, Zhang YB, Wang YG, Li BK, Yang M, Zhang XP, Liu GT (2016) Experimental evaluation of the lubrication performance of mixtures of castor oil with other vegetable oils in MQL grinding of nickel-based alloy. J Clean Prod 140:1060–1076
56. Cao JG, Wu YB, Lu D, Fujimoto M, Nomura M (2014) Material removal behavior in ultrasonic-assisted scratching of sic ceramics with a single diamond tool. Int J Mach Tools Manuf 79(4):49–61
57. Xiao XZ, Zheng K, Liao WH, Meng H (2016) Study on cutting force model in ultrasonic vibration assisted side grinding of zirconia ceramics. Int J Mach Tools Manuf 104:58–67
58. Yin QA, Li CH, Zhang YB, Yang M, Jia DZ, Hou YL, Li RZ, Dong L (2018, 2018) Spectral analysis and power spectral density evaluation in Al_2O_3, nanofluid minimum quantity lubrication milling of 45 steel. Int J Adv Manuf Technol:1–17
59. Zhang XP, Li CH, Zhang YB, Jia DZ, Li BK, Wang YG, Yang M, Hou YL, Zhang XW (2016) Performances of Al_2O_3/SiC hybrid nanofluids in minimum-quantity lubrication grinding. Int J Adv Manuf Technol 86:3427–3441
60. Zhang JC, Li CH, Zhang YB, Yang M, Jia DZ, Hou YL, Li RZ (2018) Temperature field model and experimental verification on cryogenic air nanofluid minimum quantity lubrication grinding. Int J Adv Manuf Technol 2:1–20
61. Guo C, Zhu XJ, Liu GD, Wang JQ (2015) Dynamics of cavitation bubble and parameters under ultrasonic vibration honing. J Appl Acoust 34(1):51–57
62. Jiang H, Meng X, Shen M, Peng X (2015) Hydrodynamic lubrication performance of lip seal with inclined micropores manufactured on rotary shaft surface. CIESC J 66(2):678–686
63. Jiang HS, Meng XK, Shen MX, Peng X (2017) Analysis of lip seal pumping rate enhanced by the rotary shaft surface with elliptical micro-texture. J Jiaxing Univ (6)